

Patched Completed Local Binary Pattern is an Effective Method for Neuroblastoma Histological Image Classification

Abstract

Neuroblastoma is the most common extra cranial solid tumour in children. The histology of neuroblastoma has high intra-class variation, which misleads existing computer-aided histological image classification methods that use global features. To tackle this problem, we propose a new Patched Completed Local Binary Pattern (PCLBP) method combining Sign Binary Pattern (SBP) and Magnitude Binary Pattern (MBP) within local patches to build feature vectors which are classified by k-Nearest Neighbor (k-NN) and Support Vector Machine (SVM) classifiers. The advantage of our method is extracting local features which are more robust to intra-class variation compared to global ones. We gathered a database of 1043 histologic images of neuroblastic tumours classified into five subtypes. Our experiments show the proposed method improves the weighted average F-measure by 1.89% and 0.81% with k-NN and SVM classifiers, respectively.

Keywords: neuroblastic tumour, neuroblastoma, classification, binary pattern, local patch, image analysis, computer-aided diagnosis (CAD)

1 Introduction

Neuroblastoma is the most common extra cranial solid tumour in children less than five years of age. More than 15% of childhood cancer deaths are the result of neuroblastic tumours (Park et al. 2008). Optimal management of neuroblastic tumours depends on many factors, including histopathological classification. Histological classification is performed by a medical laboratory doctor who diagnoses tumours by examining thin slices of tissue on a glass slide using an optical microscope. Pathologists commonly use the Shimada system (Shimada et al. 1999) which identifies six morphologic categories of neuroblastic tumour. Computer image analysis of tumours has been shown to improve diagnostic efficiency and consistency (Hipp et al. 2011), and identify previously unrecognized image features that predict prognosis (Yu et al. 2016). Existing methods of computer-aided diagnosis (CAD) for classification of histological images, thin slices of tissue mounted on a glass slide and viewed with a microscope, are divided into two categories: segmentation-based methods and feature-based methods. Segmentation-based methods rely on morphological features such as symmetry. Feature-based methods try to extract mathematical features from the histological images and classify them without segmentation (Boucheron 2008).

There are several factors that hinder the classification of neuroblastoma histological images based

on segmentation methods. First of all, different cells in neuroblastoma histopathological images have variations in illumination. Second, they have different shapes within the same classification group which show the high intra-class variation of neuroblastoma. In general, classification methods using segmentation may fail to detect nuclei and the different cells in images because they segment different cells based on illumination and shape. All existing feature-based classification methods used global features, extracted from the whole image, which are sensitive to intra-class variations. To our best knowledge, there is no feature-based method to address the intra-class variation problem in neuroblastoma histological image classification.

This paper proposes a local feature extraction method for classification of neuroblastoma histological images to tackle the intra-class variation problem. The contributions of this paper are:

1. We develop Patched Completed Local Binary Pattern (PCLBP) based on Completed Local Binary Pattern (CLBP) (Guo et al. 2010) for classification of neuroblastoma histological images with intra-class variation.
2. We apply PCLBP on neuroblastoma histological images with a complex histology to classify them into five different categories.
3. We evaluate our method by comparing with a state-of-the-art benchmark which shows the effectiveness of our method in the classification of neuroblastoma histological images.

The rest of this paper is as follows. Section 2 presents related work. Section 3 describes the gathered dataset. Section 4 presents the proposed Patch Completed Local Binary Pattern. Section 5 shows the experimental results. Section 6 presents the discussion and finally Section 7 concludes the work.

2 Related Work

Most proposed techniques for classification of histological images rely on morphological features (Veta et al. 2014). However, variability of illumination and appearance of different cells in the images makes classification based on segmentation more challenging. Lee & Street (2003) proposed an automated system for segmentation and classification of breast cancer’s nuclei. Mohammed et al. (2013) segmented blood cell images using watershed technique to identify chronic lymphocytic leukemia by extraction of nucleus and cytoplasm mask. Cosatto et al. (2008) classified breast cancer images using nuclei shape and size. Nguyen et al. (2011) classified nuclei into normal and cancer based on appearance and identified

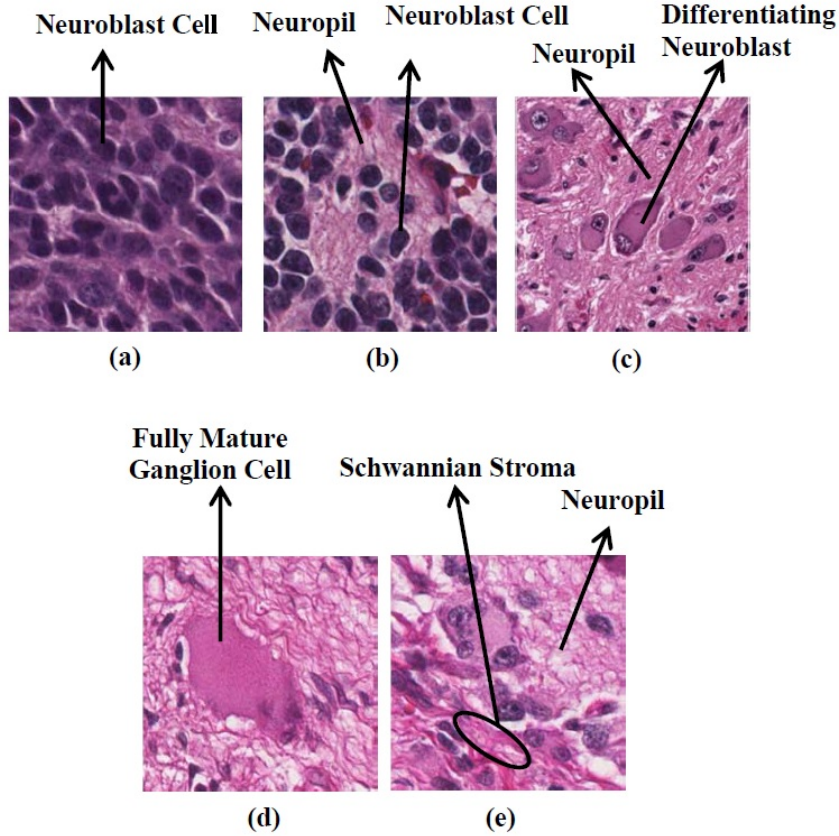


Figure 1: Neuroblastic tumour categories: (a) undifferentiated neuroblastoma, (b) poorly-differentiated neuroblastoma, (c) differentiating neuroblastoma, (d) ganglioneuroma, and (e) ganglioneuroblastoma

the cancer glands in prostate cancer. Sharma et al. (2015) segmented nuclei and classified with AdaBoost based on intensity and morphological features of nuclei.

Kong et al. (2009) classified neuroblastoma into three categories: undifferentiated, poorly-differentiated, and differentiating. They segmented the images at each resolution level into cellular, neuropil, and background elements and classified neuroblastoma histological images by integrating classifiers such as Linear Discriminative Analysis (LDA) (Lehmann 1998), Support Vector Machine (SVM) (Cortes & Vapnik 1995), and k -Nearest Neighbor (k -NN) (Cover & Hart 1967). Tafavogh et al. (2014) proposed a four stage algorithm to classify neuroblastoma tumour images into undifferentiated and poorly-differentiated using the Otsu segmentation technique (Otsu 1979). The whole slide image was partitioned. Intensity variation was reduced using an image enhancement technique, regions of interest were segmented by thresholding techniques and histological images were classified using rules based on the Shimada scheme.

In some applications, feature extraction has been used to classify histological images. All of the existing methods extracted global features which are sensitive to intra-class variation. Tabesh et al. (2007) classified prostate tissue into tumour and non-tumour based on color, texture, and morphologic features. Qureshi et al. (2008) classified meningioma using wavelet package transform and Local Binary Patterns (Ojala et al. 2002). Zhang et al. (2013) used a combination of curvelet transform, gray level co-occurrence matrix, and the Completed Local Binary Patterns (CLBP) as features to stratify breast cancer tumours from histo-

logical images. Farjam et al. (2007) used texture features to identify the glandular elements within images of prostate tissue. They applied k -means to cluster the image components. Spanhol et al. (2016) applied a completed modeling of the Local Binary Pattern (LBP), based on three components extracted from the 8-neighborhood: center pixel, sign, and magnitude. The center pixel is coded into a binary bit after global thresholding. The difference signs and magnitudes are coded in binary format so that they can be combined to form the final Completed Local Binary Pattern histograms. Spanhol et al. (2016) used the combination of Completed Local Binary Patterns with k -NN and SVM to classify a large dataset of breast cancer histological images into benign and malignant classes. Classification of neuroblastoma histological images remains challenging due to the intra-class variation.

3 Dataset

There is a lack of large and publicly available image datasets for analysis of neuroblastic tumours, which significantly hinders development and validation of methods. Therefore, we gathered a dataset of images from neuroblastic tumours. Tumour access is compliant with local policy, national legislation, and ethical mandates to use the human tissue in research. All patient specific details were removed and a de-identified dataset was used for this research. The initial dataset consisted of images of tissue microarrays (TMA) of neuroblastic tumours, scanned by the Aperio ScanScope system. Each slide was composed of 20 to 40 1.2mm cores of neuroblastic tumour, stained with haematoxylin and eosin (H&E) and cut

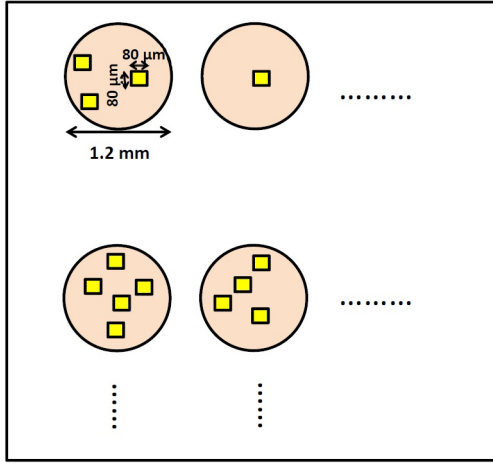


Figure 2: Quantitative actual size of tissue spots and cropped images

Table 1: Number of different categories of neuroblastic tumour cropped images

Category of Neuroblastic Tumour	Number of Cropped Images	Number of Patients
poorly-differentiated	571	77
differentiating	187	12
undifferentiated	155	10
ganglioneuroma	84	18
ganglioneuroblastoma	46	8
Total	1043	125

at $3\mu\text{m}$. In this method, the contrast between different cells which have different colors is increased. Staining with H&E allows observation of histological structures. TMA images were in svf format with resolution $0.2\mu\text{m}$, images were viewed and extracted using ImageScope software (*ImageScope* 2016). Tissue cores were classified by experts into five different categories: poorly-differentiated, differentiating, undifferentiated, ganglioneuroma, and ganglioneuroblastoma, according to the Shimada classification system. Representative images in the categories are shown in Figure 1.

Areas best representative of each category, and devoid of artefacts, were selected from each tissue core by an expert histopathologist. At $40\times$ magnification, cropped image size was 300×300 pixels with real size $80\times 80\mu\text{m}$ which is approximately one third of the area of an optical microscope high power field of view. Figure 2 shows the quantitative actual size of tissue spots and cropped images.

This size was chosen as a compromise between being large enough to capture diagnostic features of each category and small enough for computational cost. Numbers of images in our dataset are given in Table 1. It is much larger in terms of patients and images than the datasets used by Tafavogh et al. (2014) and Kong et al. (2009). Moreover, the intra-class variation of neuroblastoma cells in the gathered dataset is very high which means different cells in neuroblastoma histological images within the same patients in the same class have different shapes. An example of the high intra-class variation of differentiating neuroblastoma is shown in Figure 3. As can be seen, both of them are differentiating type but their cells have different shapes.

4 Patch Completed Local Binary Pattern (PCLBP)

Before describing our PCLBP algorithm, we first describe the algorithm it is based on Completed Local Binary Pattern (CLBP) is one of the latest variants of Local Binary Pattern (LBP) (Ojala et al. 2002). The LBP operator computes the distribution of binary patterns in the circular neighborhood characterized by a radius R and a number of neighbors P . The idea is to threshold neighboring pixels, compared to the central pixel to the P neighbors. If the intensity of a neighbor pixel is greater than or equal to that of the central pixel the value 1 is assigned, otherwise 0. Therefore, a binary pattern is obtained from the neighborhood. The LBP function at pixel p is (from (Ojala et al. 2002))

$$LBP(f(X, Y)) = \sum_{i=0}^{P-1} 2^i \cdot u(f(X_i, Y_i) - f(X, Y)) \quad (1)$$

where $f(X_i, Y_i)$ and $f(X, Y)$ are grey levels of pixels (X_i, Y_i) and (X, Y) and $u(\cdot)$ is the unit step function. The CLBP is a completed modeling of LBP (Guo et al. 2010) which is based on three components extracted from the local region: center pixel, sign, and magnitude. The center pixel is coded by a binary code after thresholding, with the threshold set as the average grey level of the whole image. For computing the sign and magnitude, a neighborhood of radius R and number of neighbors P is considered. Signs and magnitudes are computed and coded by a specific operator into the binary format so that they can be combined to form the final CLBP histograms (Guo

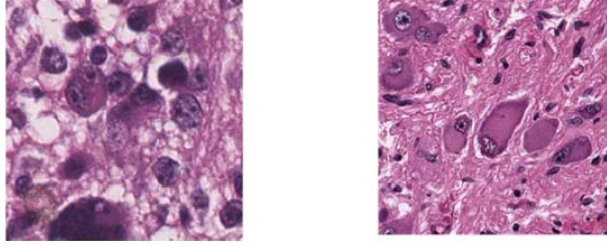


Figure 3: An example of high intra-class variation of differentiating neuroblastoma

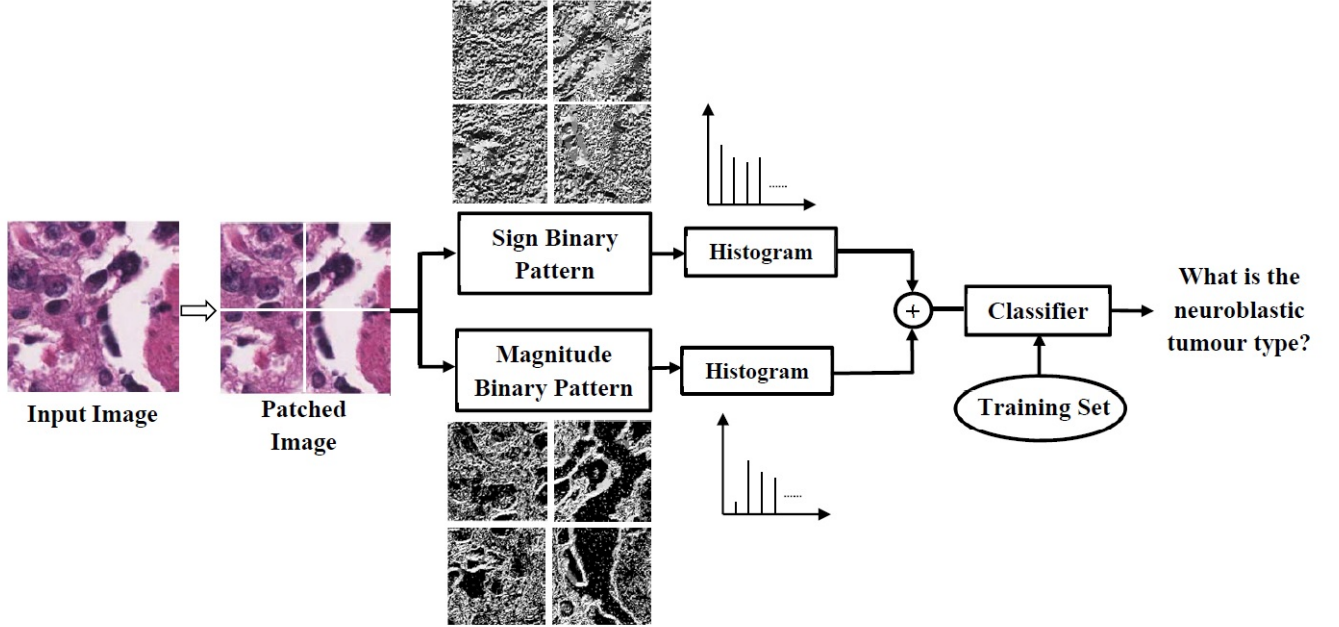


Figure 4: The scheme of the proposed method

et al. 2010).

Our approach, Patched Completed Local Binary Pattern (PCLBP), extends CLBP. The overall framework consists of four stages as shown in Figure 4. First, the images are partitioned into equal-sized square patches. Second, Sign Binary Patterns (SBPs) and Magnitude Binary Patterns (MBPs) are computed within patches. Third, histograms of SBPs and MBPs are computed and concatenated to build a feature vector for each patch. A feature vector for the whole image is created by concatenating the feature vectors of all patches. Finally, the input image is classified by comparing the related feature vector with the feature vectors of all images in the gallery. Following we describe the algorithm in detail.

Given an $N \times N$ pixel input image, we partition it into $W \times W$ pixel non-overlapping patches. We indicate all points in the patch with p and q indices, ranging from 1 to N/W , as

$$p = \left\lfloor \frac{X}{W} \right\rfloor + 1, \quad q = \left\lfloor \frac{Y}{W} \right\rfloor + 1 \quad (2)$$

where $0 \leq X \leq N$ and $0 \leq Y \leq N$ are the coordinates of the input neuroblastoma image and $\lfloor \cdot \rfloor$ is the floor function. The (p,q) th patch in the input neuroblastoma image (see Figure 5) is defined as

$$f_{p,q}(X^{pq}, Y^{pq}) = f(W(p-1)+X^{pq}, W(q-1)+Y^{pq}) \quad (3)$$

where $f(X,Y)$ denotes the original image. X^{pq}, Y^{pq} denote the coordinate of the (p,q) th patch.

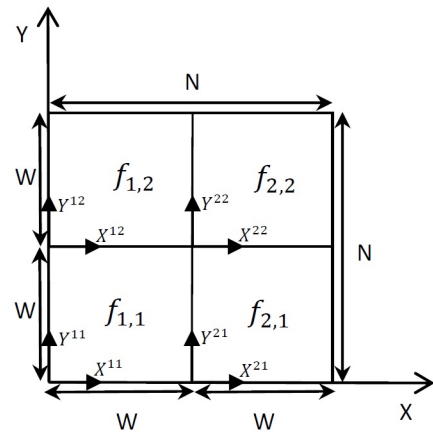


Figure 5: Coordinates in the patched image. Here, we assume $W = N/2$

The local differences of the 8-neighborhood around (X_0^{pq}, Y_0^{pq}) , see Figure 6, are computed as

$$f'_{p,q,k}(X_0^{pq}, Y_0^{pq}) = f_{p,q}(X_k^{pq}, Y_k^{pq}) - f_{p,q}(X_0^{pq}, Y_0^{pq}); k = 1, \dots, 8 \quad (4)$$

(X_1^{pq}, Y_1^{pq})	(X_2^{pq}, Y_2^{pq})	(X_3^{pq}, Y_3^{pq})
(X_8^{pq}, Y_8^{pq})	(X_0^{pq}, Y_0^{pq})	(X_4^{pq}, Y_4^{pq})
(X_7^{pq}, Y_7^{pq})	(X_6^{pq}, Y_6^{pq})	(X_5^{pq}, Y_5^{pq})

Figure 6: An 8-neighborhood around (X_0^{pq}, Y_0^{pq})

The SBP of the (p,q) th patch, $SBP_{p,q}(f_{p,q}(X_0^{pq}, Y_0^{pq}))$, is defined as the concatenation of 8 bits as

$$SBP_{p,q}(f_{p,q}(X_0^{pq}, Y_0^{pq})) = \{u(f'_{p,q,1}(X_0^{pq}, Y_0^{pq})), \dots, u(f'_{p,q,8}(X_0^{pq}, Y_0^{pq}))\} \quad (5)$$

where $u(x)$ is the unit step function:

$$u(x) = \begin{cases} 1 & \text{if } x \geq 0 \\ 0 & \text{if } x < 0 \end{cases} \quad (6)$$

and the MBP for the (p,q) th patch is defined as

$$MBP_{p,q}(f_{p,q}(X_0^{pq}, Y_0^{pq})) = \{u(f'_{p,q,1}(X_0^{pq}, Y_0^{pq}) - m), \dots, u(f'_{p,q,8}(X_0^{pq}, Y_0^{pq}) - m)\} \quad (7)$$

where m is a threshold to be set as the average of the absolute values of all derivatives in the neuroblastoma image.

After computing the SBP and the MBP, they are converted into decimal values as

$$DSBP_{p,q}(f_{p,q}(X_0^{pq}, Y_0^{pq})) = \sum_{l=1}^8 2^{l-1} SBP_{p,q}^l(f_{p,q}(X_0^{pq}, Y_0^{pq})) \quad (8)$$

$$DMBP_{p,q}(f_{p,q}(X_0^{pq}, Y_0^{pq})) = \sum_{l=1}^8 2^{l-1} MBP_{p,q}^l(f_{p,q}(X_0^{pq}, Y_0^{pq})) \quad (9)$$

where $SBP_{p,q}^l(f_{p,q}(X_0^{pq}, Y_0^{pq}))$ and $MBP_{p,q}^l(f_{p,q}(X_0^{pq}, Y_0^{pq}))$ denotes the l -th bit of the SBP and the MBP, respectively. DSBP and DMBP for each pixel in the neuroblastoma image are computed. Figure 7 shows an example of DMBP

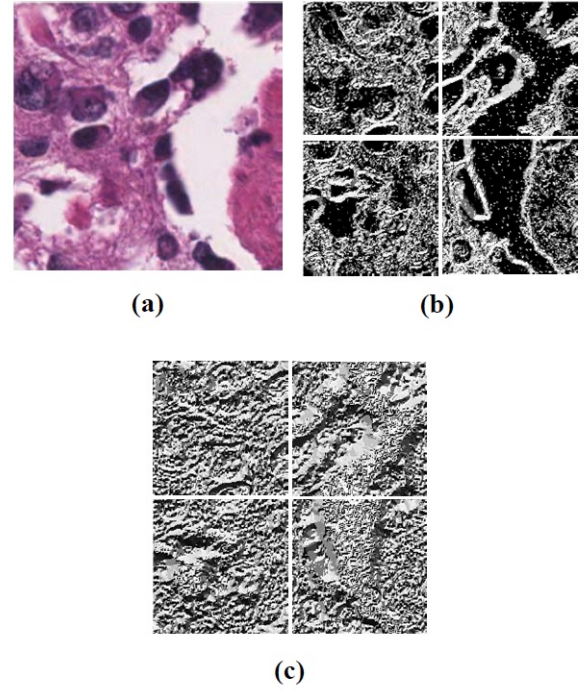


Figure 7: An example of computed Magnitude Binary Pattern (MBP) and Sign Binary Pattern (SBP): (a) original image, (b) MBP, and (c) SBP. The optimal patch size (W) is 60 Pixels. Here, we assume $W = 150$ pixels for better visualization.

and DSBP in an arbitrary neuroblastoma image. For each patch, we model the distribution of DSBP and DMBP using the histogram operator with 256 bins as

$$HSBP_{p,q}(f_{p,q}(X, Y)) = H\{DSBP_{p,q}(f_{p,q}(X, Y))\} \quad (10)$$

$$HMBP_{p,q}(f_{p,q}(X, Y)) = H\{DMBP_{p,q}(f_{p,q}(X, Y))\} \quad (11)$$

We concatenate the histograms of the SBP and the MBP for each patch to build a Local Histogram (LH) for each patch

$$LH_{p,q}(f_{p,q}(x, y)) = \{HSBP_{p,q}(f_{p,q}(x, y)), HMBP_{p,q}(f_{p,q}(x, y))\} \quad (12)$$

Then, we concatenate the histograms of all patches to build the Patch Completed Local Binary Pattern for the neuroblastoma image (as shown in Figure 8)

$$PCLBP = \{LH_{p,q}(f_{p,q}(X, Y)) | p, q = 1, \dots, N/W\} \quad (13)$$

Finally, two algorithms are used to classify the extracted PCLBPs: k -NN (Cover & Hart 1967) and SVM (Cortes & Vapnik 1995).

5 Experimental Results

In this section, we evaluate the performance of the proposed method for classification of neuroblastoma histological images. Experiments are conducted on the collected neuroblastic tumour database.

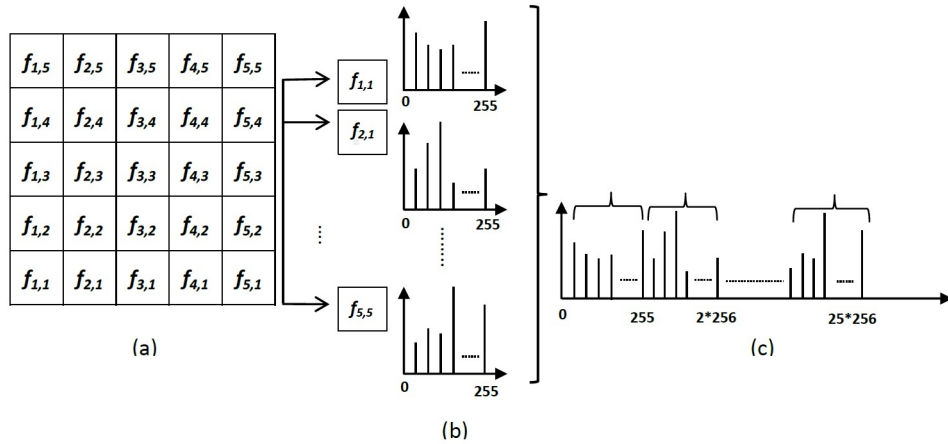


Figure 8: Concatenation of patches' histograms: (a) patched image, (b) histogram of patches, and (c) concatenation of patches' histograms.

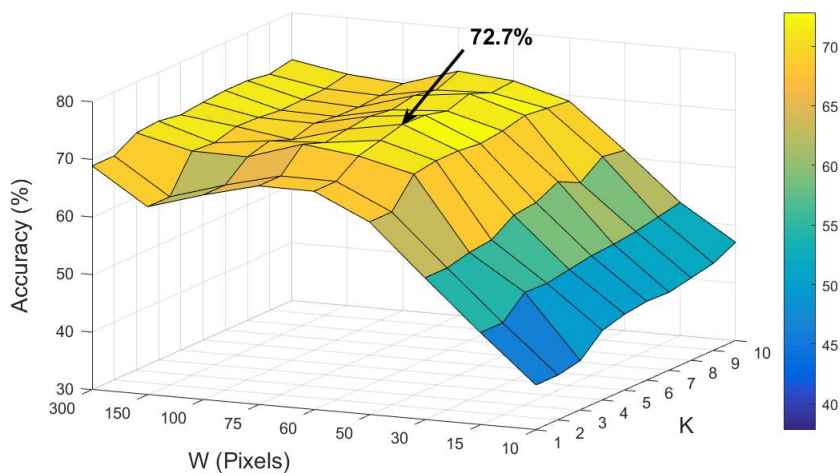


Figure 9: Accuracy of k -NN classifier versus patch width (W) and k in parameter tuning of k -NN classifier

The database is divided randomly into two subsets: parameter-tuning (211 images) and validation datasets (832 images). We select the optimum values for free parameters using the training dataset and fix them for the validation. Then, we evaluate the system using the validation dataset and selected parameters.

5.1 Parameter Tuning

We divide the parameter-tuning dataset into training (150 images) and testing (61 images) subsets. We train the algorithm using the training set with different parameter values, test using the testing set and compute the accuracies. To have a better estimation of the accuracy, we repeat the above procedure multiple (10) times and compute the average over all experiments.

For k -NN, the free parameters are the width of the patch (W) and the k numbers of neighbours. Accuracy was computed for k ranging from 1 to 10 and patch width $W \in \{10, 15, 30, 50, 60, 75, 100, 150, 300\}$ and the results are shown in Figure 9. Best accuracy of 72.7% was found with $W=60$ and $k=5$. So we used these values in the next experiments.

For SVM, we used the C-SVC type (Boser et al. 1992) using LIBSVM tool (Chang & Lin 2011) and tested different kernels: linear, polynomial, Radial Basis Function (RBF), and sigmoid. Table 2 shows

accuracies using different kernels. As can be seen, the best result is achieved using the RBF kernel, so we selected it for the next experiments. RBF parameter γ was empirically defined through experiments with best value taking $1/256$ (256 is the number of different intensities in the images).

Table 2: Average classification accuracy of SVM over neuroblastic tumour dataset using different kernel functions

Kernel	Classification Accuracy (%)
Linear	62.22
Polynomial	71.82
Radial Basis Function	72.33
Sigmoid	49.45

5.2 System Validation

Here, we use the remaining 80% of the dataset which is not seen in the parameter tuning phase. It is divided into training (623 images) and validation (209

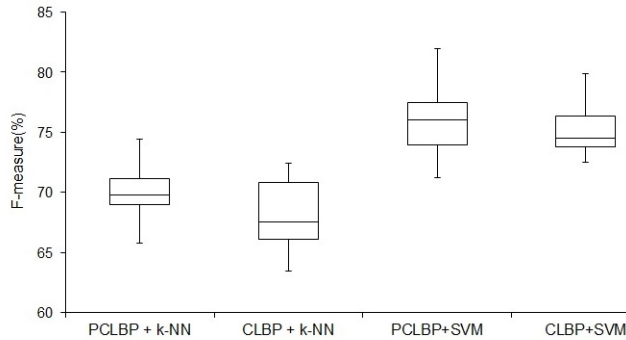


Figure 10: Comparison between our algorithm (PCLBP) and Spanhol’s system (CLBP)

Table 3: Weighted average precision, recall, and F-measure obtained by our system and Spanhol’s system.

	Our system (PCLBP)(%)	Spanhol’s system (CLBP)(%)
Precision-kNN	70.49±3.37	68.22±3.23
Precision-SVM	75.59±3.15	74.1±2.35
Recall-kNN	71.02±2.87	69.53±2.81
Recall-SVM	76.35±3.41	76.25±2.23
F-measure-kNN	70.75±3.09	68.86±6.04
F-measure-SVM	75.96±3.27	75.15±2.28

images) sets. We train the algorithm using the training set (with the parameter values selected in Section 5.1) and test using the validation set. We repeat this procedure multiple (10) times and report the average accuracy. Algorithm performance for k -NN and SVM is reported with the average F-measure, recall, and precision (Powers 2011) weighted by number of examples in each of the five classes. Distribution of the computed F-measures for the two classifiers and feature extraction approaches over the ten trials is presented in Figure 10 and shows that SVM works better than k -NN. The t -test with P value = 0.03 and $\alpha=0.05$ (significance level) shows that combination of our algorithm with SVM classifier significantly improves the accuracy of classification in comparison with k -NN classifier. Table 3 indicates that our algorithm obtains approximately 5% higher accuracy when it is combined with SVM classifier compared to the k -NN classifier. We also test the CLBP algorithm (Spanhol et al. 2016) on the test images as a benchmark, again reporting the weighted average of precision, recall, and F-measure. Table 3 reports the weighted average precision, recall, and F-measure of our system and Spanhol’s system. The weighted average precision, recall, and F-measure of our system are better than Spanhol’s system.

6 Discussion

The proposed algorithm is a new feature extraction method to classify neuroblastoma histological images into five different groups. Although a large number of methods have been proposed in the literature, our system has multiple advantages over these systems:

1. There is no feature based method to classify histological images into more than two categories. They were classified more straightforward to binary classification. However, the proposed method can classify neuroblastoma tumour im-

ages to five different categories.

2. Neuroblastoma has a complex texture with a great deal of complicated features compared to other types of cancer such as breast cancer. It is the first time that neuroblastoma histological images are classified into five different categories using a feature extraction method.
3. The proposed method extract features within small patches which are not easily detected by human eyes.

7 Conclusion

We proposed a new Patched Completed Local Binary Pattern (PCLBP) to classify neuroblastic tumours into five different categories using extracted feature vectors from histological images. The algorithm built the feature vector by extraction of SBP and MBP within local patches. The advantage of the proposed method is extraction of local features which are more robust to intra-class variation compared to global feature extraction. The evaluation was conducted on a gathered dataset with 1043 cropped images from samples of five different categories. We compare the results obtained by our system with the state-of-the-art. Results indicate that the proposed method has improved the average weighted F-measure for k -NN and SVM by 1.89% and 0.81%, respectively, compared to the benchmark.

References

- Boser, B., Guyon, I. & Vapnik, V. (1992), A Training Algorithm for Optimal Margin Classifiers, in ‘Proceedings of the Fifth Annual Workshop on Computational Learning Theory’, pp. 144–152.
- Boucheron, L. (2008), *Object-and Spatial-Level Quantitative Analysis of Multispectral Histopathology*

- Images for Detection and Characterization of Cancer*, Doctoral Dissertation in University of California at Santa Barbara.
- Chang, C. & Lin, C. (2011), 'LIBSVM: A Library for Support Vector Machines', *ACM Transactions on Intelligent Systems and Technology (TIST)* **2**(3), 1–27. Software available at <http://www.csie.ntu.edu.tw/~cjlin/libsvm>.
- Cortes, C. & Vapnik, V. (1995), 'Support-Vector Networks', *Machine Learning* **20**(3), 273–297.
- Cosatto, E., Miller, M., Graf, H. & Meyer, J. (2008), Grading Nuclear Pleomorphism on Histological Micrographs, in 'International Conference on Pattern Recognition', pp. 1–4.
- Cover, T. & Hart, P. (1967), 'Nearest Neighbor Pattern Classification', *IEEE Transactions on Information Theory* **13**(1), 21–27.
- Farjam, R., Soltanian-Zadeh, H., Jafari-Khouzani, K. & Zoroofi, R. (2007), 'An Image Analysis Approach for Automatic Malignancy Determination of Prostate Pathological Images', *Cytometry Part B: Clinical Cytometry* **72**(4), 227–240.
- Guo, Z., Zhang, L. & Zhang, D. (2010), 'A Completed Modeling of Local Binary Pattern Operator for Texture Classification', *IEEE Transactions on Image Processing* **19**(6), 1657–1663.
- Hipp, J., Flotte, T., Monaco, J., Cheng, J., Madabhushi, A., Yagi, Y., Rodriguez-Canales, J., Emmert-Buck, M., Dugan, M., Hewitt, S., Toner, M., Tompkins, R., Lucas, D., Gilbertson, J. & Balis, U. (2011), 'Computer-Aided Diagnostic Tools Aim to Empower Rather than Replace Pathologists: Lessons Learned from Computational Chess', *Journal of Pathology Informatics* **2**(1), 25–25.
- ImageScope (2016).
URL: <http://www.leicabiosystems.com/digital-pathology/digital-pathology-management/imagescope/>
- Kong, J., Sertel, O., Shimada, H., Boyer, K., Saltz, J. & Gurcan, M. (2009), 'Computer-Aided Evaluation of Neuroblastoma on Whole-Slide Histology Images: Classifying Grade of Neuroblastic Differentiation', *Pattern Recognition* **42**(6), 1080–1092.
- Lee, K. & Street, W. (2003), 'An Adaptive Resource-Allocating Network for Automated Detection, Segmentation, and Classification of Breast Cancer Nuclei Topic Area: Image Processing and Recognition', *IEEE Transactions on Neural Networks* **14**(3), 680–687.
- Lehmann, E. (1998), *Theory of Point Estimation*, Springer.
- Mohammed, E., Mohamed, M., Naugler, C. & Far, B. (2013), Chronic Lymphocytic Leukemia Cell Segmentation from Microscopic Blood Images using Watershed Algorithm and Optimal Thresholding, in '26th IEEE Canadian Conference on Electrical and Computer Engineering', pp. 1–5.
- Nguyen, K., Jain, A. & Sabata, B. (2011), 'Prostate Cancer Detection: Fusion of Cytological and Textural Features', *Journal of Pathology Informatics* **2**:S3.
- Ojala, T., Pietikainen, M. & Maenpaa, T. (2002), 'Multiresolution Gray-Scale and Rotation Invariant Texture Classification with Local Binary Patterns', *IEEE Transactions on Pattern Analysis and Machine Intelligence* **24**(7), 971–987.
- Otsu, N. (1979), 'A Threshold Selection Method from Gray-Level Histograms', *IEEE Transactions on Systems, Man, and Cybernetics* **9**(1), 62–66.
- Park, J., Caron, H. & Eggert, A. (2008), 'Neuroblastoma: Biology, Prognosis, and Treatment', *Pediatric Clinics of North America* **55**(1), 97–120.
- Powers, D. (2011), 'Evaluation: from precision, recall and f-measure to roc, informedness, markedness, and correlation', *Journal of Machine Learning Technologies* **2**(1), 37–63.
- Qureshi, H., Sertel, O., Rajpoot, N., Wilson, R. & Gurcan, M. (2008), Adaptive Discriminant Wavelet Packet Transform and Local Binary Patterns for Meningioma Subtype Classification, in 'Proceedings of the 11th International Conference on Medical Image Computing and Computer-Assisted Intervention, Part II', pp. 196–204.
- Sharma, H., Zerbe, N., Heim, D., Wienert, S., Behrens, H., Hellwich, O. & Hufnagl, P. (2015), A Multi-Resolution Approach for Combining Visual Information using Nuclei Segmentation and Classification in Histopathological Images, in '10th International Conference on Computer Vision Theory and Applications', pp. 37–46.
- Shimada, H., Ambros, I., Dehner, L., Hata, J., Joshi, V., Roald, B., Stram, D., Gerbing, R., Lukens, J., Matthay, K. & Castleberry, R. (1999), 'The International Neuroblastoma Pathology Classification (the Shimada System)', *Cancer* **86**(2), 364–372.
- Spanhol, F., Oliveira, L., Caroline, P. & Laurent, H. (2016), 'A Dataset for Breast Cancer Histopathological Image Classification', *IEEE Transactions on Biomedical Engineering* **63**(7), 1455–1462.
- Tabesh, A., Teverovskiy, M., Pang, H., Kumar, V., Verbel, D., Kotsianti, A. & Saidi, O. (2007), 'Multifeature Prostate Cancer Diagnosis and Gleason Grading of Histological Images', *IEEE Transactions on Medical Imaging* **26**(10), 1366–1378.
- Tafavogh, S., Meng, Q., Catchpoole, D. & Kennedy, P. (2014), Automated quantitative and qualitative analysis of the whole slide images of neuroblastoma tumour for making a prognosis decision, in 'Proceedings of the IASTED 11th International Conference on Biomedical Engineering', pp. 244–251.
- Veta, M., Pluim, J., van Diest, P. & Viergever, M. (2014), 'Breast Cancer Histopathology Image Analysis: A Review', *IEEE Transactions Biomed Eng.* **61**(5), 1400–1411.
- Yu, K., Zhang, C., Berry, G., Altman, R., Re, C., Rubin, D. & Snyder, M. (2016), 'Predicting Non-Small Cell Lung Cancer Prognosis by Fully Automated Microscopic Pathology Image Features', *Nature Communications* **7**, 1–10.
- Zhang, Y., Zhang, B. & Lu, W. (2013), 'Breast Cancer Histological Image Classification with Multiple Features and Random Subspace Classifier Ensemble', *Studies in Computational Intelligence* **450**, 27–42.